PERGAMON

International Journal of Solids and Structures 38 (2001) 2615–2637

INTERNATIONAL JOURNAL OF SOLIDS and STRUCTURES

www.elsevier.com/locate/ijsolstr

Taylor-based nonlocal theory of plasticity

Huajian Gao [a,*], Yonggang Huang [b]

[a] *Department of Mechanical Engineering, Division of Mechanics and Computation, Stanford University, Stanford, CA 94305, USA*
[b] *Department of Mechanical and Industrial Engineering, University of Illinois, Urbana, IL 61801, USA*

Received 28 December 1999; in revised form 20 April 2000

Abstract

A Taylor-based nonlocal theory of plasticity is proposed to account for the size dependence of plastic deformation at micron and submicron length scales. This theory is intended to link Taylor's model of dislocation hardening to a nonlocal theory of plasticity in which the density of geometrically necessary dislocations is expressed as a nonlocal integral of the strain field. We make application of this theory to void growth, cavitation instabilities and particle-reinforced composites, as well as comparison with experiments on micro-torsion, micro-bending and micro-indentation.

Keywords: Plasticity; Non-local theory; Strain gradient plasticity; Dislocations; Strengthening mechanics; Consitutive theory

1. Introduction

There is mounting experimental evidence that materials display strong size effects when the characteristic length scale associated with nonuniform plastic deformation is on the order of microns. Fleck et al. (1994) conducted micro-twisting of thin copper wires and reported an increase by a factor of 3 in the normalized shear strength as the wire diameter decreases from 170 to 12 μm while the increase of work-hardening in simple tension of the same wires is negligible. Stolken and Evans (1998) investigated micro-bending of thin nickel beams and observed a similar magnitude of increase in the normalized bending strength as the beam thickness decreases from 100 to 12.5 μm. Lloyd (1994) studied metal matrix composites such as aluminum–magnesium matrix reinforced by silicon carbide particles and observed a substantial strength increase as the particle diameter was reduced from 16 to 7.5 μm with the particle volume fraction fixed at 15%. Similar size dependence of the metal matrix composites has also been observed by Nan and Clarke (1996). In micro-indentation tests of various metallic materials, the measured indentation hardness increases by a factor of two as the depth of indentation decreases from 10 to 1 μm (Nix, 1989; De Guzman et al., 1993; Stelmashenko et al., 1993; Ma and Clarke, 1995; Poole et al., 1996; McElhaney et al., 1998).

Size-dependent plasticity may also be important in explaining the fracture behavior of ductile materials. Elssner et al. (1994) measured both the macroscopic fracture toughness and atomic work of separation of

* Corresponding author. Fax: +1-650-723-1778.
E-mail address: gao@am-sun2.stanford.edu (H. Gao).

0020-7683/01/$ - see front matter
PII: S0020-7683(00)00173-6

an interface between a single crystal of niobium and a sapphire single crystal. The macroscopic work of fracture was measured using a four-point bend specimen designed for the determination of interfacial toughness, while the atomic work was inferred from the equilibrium shapes of microscopic pores on the interface. The interface between the two materials remained atomistically sharp, i.e. the crack tip was not blunted even though niobium is ductile and has a large number of dislocations. The stress level needed to produce atomic decohesion of a lattice or a strong interface is typically on the order of 3% of Young's modulus, or 10 times the tensile yield stress. Hutchinson (1997) pointed out that the maximum stress level that can be achieved near a crack tip cannot reach higher than four to five times the tensile yield strength of metals, according to models based on conventional plasticity theories. This clearly falls short of triggering the atomic decohesion observed in the experiments of Elssner et al. (1994). The linkage between macroscopic cracking and atomistic fracture is crucially important in predicting adhesion strength and fracture toughness of multilayer structures in microelectronic devices (Dauskardt et al., 1998).

Classical theories of plasticity possess no internal length scale and cannot explain the size dependence of plasticity observed in experiments. From a microscopic point of view, plastic deformation in metallic materials reflects the collective behavior of a vast number of dislocations. When a material is deformed, dislocations are generated, moved, and stored, and the storage causes the material to work harden. Dislocations become stored for one of the two reasons: they accumulate by trapping each other in a random way, or they are required for compatible deformation of various parts of the material. In the former case the dislocations are referred to as statistically stored dislocations (Ashby, 1970), while in the latter case, they are called geometrically necessary dislocations.

Geometrically necessary dislocations can be related to the gradients of plastic strain in a material (Nye, 1953; Cottrell, 1964; Ashby, 1970). This consideration has motivated Fleck and Hutchinson (1993, 1997) and Fleck et al. (1994) to develop a phenomenological theory of strain gradient plasticity within the mathematical framework of higher-order continuum theories of elasticity (Toupin, 1962; Koiter, 1964; Mindlin, 1964). The importance of strain gradients in plastic deformation has also been recognized by many other researchers in the past (e.g., Kroener, 1962; Aifantis, 1984; Zbib and Aifantis, 1989a,b,c; de Borst and Muhlhaus, 1992). The phenomenological nature of these theories often leads to numerous model parameters which are difficult to be fully tested based on the limited number of micromechanical, gradient-dominant experiments. Nix and Gao (1998) found that micro-indentation experiments strongly suggest a linear dependence of the square of plastic flow stress on strain gradient. While such linear dependence is predicted by the Taylor model of dislocation hardening which relates the flow stress to dislocation density, the phenomenological strain gradient theories have not been able to explain such behavior. This has motivated Gao et al. (1999a) and Huang et al. (2000a) to develop a mechanism-based theory of strain gradient (MSG) plasticity which builds the Taylor model as a foundation into the higher-order continuum framework of Fleck and Hutchinson (1997). In comparison with phenomenological theories, the MSG theory has minimum number of adjustable parameters and gives predictions in good agreement with experiments on micro-torsion, micro-bending and micro-indentation (Gao et al., 1999b).

As strain gradient plasticity theories involve the gradient of plastic strain in the constitutive equations, the order of governing equations becomes higher such that additional boundary conditions must be imposed. A new effort is to explore alternative frameworks which could model size-dependent plasticity without higher-order stresses and strains, so as to preserve the essential structure of classical plasticity. Acharya and Bassani (2000) discussed a rate-independent framework in which the stress increments are related to strain increments via a plastic work hardening modulus that depends not only on the plastic strain, but also on the gradient of plastic strain. Dai and Parks (2000), on the other hand, have developed a rate-dependent single crystal plasticity framework in which the shear strain rate on a slip system is expressed as a power-law function of the critical resolved shear stress and the slip resistance on the given slip system. The strain gradient effects come into play through the slip resistance which increases with strain gradients according to the obstacle density that correlates with dislocation densities on all active slip systems.

In this paper, we explore the possibility of modeling size-dependent plasticity within the framework of nonlocal continuum theories. It is known that the basic balance laws in a nonlocal continuum theory are identical to classical local theories (Eringen, 1981, 1983), i.e. the order of governing equations remains the same as that of a classical theory. In comparison with a high order theory, a nonlocal theory does not require additional boundary conditions and the length scale is introduced into the constitutive equations via nonlocal variables which are expressed as an integral of local variables over all the material points in the body. Various nonlocal plasticity theories have already been used in the past (e.g., Bazant et al., 1984; Basant, 1986; Pijaudier-Cabot and Bazant, 1987; Bazant and Lin, 1988; Stromberg and Ristinmaa, 1996; Chen, 1999) to provide a length scale in the description of strain softening and damage accumulation in deformed solids. We intend to link such theories with the Taylor model of dislocation hardening and to provide a micromechanical basis for using nonlocal theories to model size-dependent plastic deformation at micron and submicron length scales.

2. Theory formulation

2.1. The micromechanical basis of size-dependent plasticity

Dislocation theory indicates that the Peach–Koehler force due to interaction of a pair of dislocations is proportional to

$$\tau_{\text{pair}} \sim \frac{\mu b}{L}, \tag{1}$$

where μ is the shear modulus, b, the Burgers vector and L, the distance between dislocations. This stress sets a critical value for the applied stress to break or untangle the interactive pair so that slip can occur even if one of the dislocation is pinned by an obstacle. This picture is generalized by the Taylor model to a group of statistically stored dislocations which trap each other in a random way. If the mean dislocation spacing is L, the critical stress required to untangle the interactive dislocations and to induce significant plastic deformation is defined as

$$\tau = \frac{\alpha \mu b}{L} = \alpha \mu b \sqrt{\rho}, \tag{2}$$

where $\rho = 1/L^2$ is the dislocation density and α, an empirical constant usually on the order of 1 (e.g., Nix and Gibeling, 1985). The Taylor flow stress can also be viewed as the 'passing stress' for a moving dislocation to glide through a forest of tangled dislocations without being pinned. The similarity between the Taylor model and the interaction of a pair of dislocations indicates the potential of using Eq. (2) as a fundamental measure of dislocation interaction at length scales close to those of discrete dislocations.

Nix and Gao (1998) generalized the Taylor relation to account for geometrically necessary dislocations

$$\tau = \alpha \mu b \sqrt{\rho_{\text{T}}} = \alpha \mu b \sqrt{\rho_{\text{S}} + \rho_{\text{G}}}, \tag{3}$$

where ρ_{T} is the total dislocation density, ρ_{S}, the density of statistically stored dislocations and ρ_{G}, the density of geometrically necessary dislocations. In writing the total obstacle density as a direct sum of ρ_{S} and ρ_{G}, the Taylor flow stress has been viewed as the 'passing stress' for a moving dislocation to glide through a forest of obstacles consisting of both the statistically stored and geometrically necessary dislocations. Nix and Gao (1998) used the von Mises rule to relate the tensile flow stress to the shear flow stress as $\sigma = \sqrt{3}\tau$, where the factor $\sqrt{3}$ results from isotropy of solids. For crystalline materials (e.g., face-centered-cubic

solids), a more accurate relationship accounting for the so-called Taylor factor (Bishop and Hill, 1951a,b; Kocks, 1970) between the tensile flow stress and critical resolved shear stress in slip systems is

$$\sigma = 3\tau = 3\alpha\mu b\sqrt{\rho_S + \rho_G}. \tag{4}$$

The density of statistically stored dislocations ρ_S can be determined (Nix and Gao, 1998) from the uniaxial stress–strain law in the absence of strain gradient effects,

$$\sigma = 3\alpha\mu b\sqrt{\rho_S} = \sigma_{ref} f(\epsilon), \tag{5}$$

where σ_{ref} is a reference stress in uniaxial tension. On the other hand, the density of geometrically necessary dislocations ρ_G can be related to an effective strain gradient η as

$$\rho_G = 2\eta/b, \tag{6}$$

where the factor of 2 is the so-called Nye factor (Arsenlis and Parks, 1999) for a polycrystalline material. The actual density of geometrically necessary dislocations depends not only on nonuniform deformation (strain gradients), but also on the orientation of slip systems. The Nye factor accounts for ratio of average density of geometrically necessary dislocations to that for the most efficient dislocation configurations considered by Gao et al. (1999a). Actually, the Nye factor may depend on the material as well as the type of external loading. Arsenlis and Parks (1999) have found the Nye factor to be 1.85 in the case of bending and 1.93 in the case of torsion of FCC polycrystals. In general, it is anticipated that the Nye factor is on the order of two for FCC polycrystals and can be as high as three for FCC single crystals (Parks, 1999).

Combining Eqs. (3)–(6) leads to a law of strain gradient plasticity (Nix and Gao, 1998),

$$\sigma = \sigma_{ref}\sqrt{f^2(\epsilon) + \ell\eta}, \tag{7}$$

where

$$\ell = 18\alpha^2\left(\frac{\mu}{\sigma_{ref}}\right)^2 b \tag{8}$$

is identified as the material length introduced by Fleck and Hutchinson (1993, 1997). A typical estimate of ℓ is on the order of a few microns.

In order to develop a constitutive law based on Eq. (7), the density of geometrically necessary dislocations ρ_G must be related to the strain gradient tensor

$$\eta_{ijk} = u_{k,ij} = \epsilon_{ik,j} + \epsilon_{jk,i} - \epsilon_{ij,k}, \tag{9}$$

where u_k and ϵ_{ij} denote the displacements and strains, respectively. Following Fleck and Hutchinson (1997), Gao et al. (1999a) defined

$$\eta = \sqrt{c_1\eta'_{iik}\eta'_{jjk} + c_2\eta'_{ijk}\eta'_{ijk} + c_3\eta'_{ijk}\eta'_{kji}} \tag{10}$$

as an effective strain gradient which measures the density of geometrically necessary dislocations as $\rho_G = 2\eta/b$; the three constants c_1, c_2, and c_3 scale the three quadratic invariants for the third order deviatoric strain gradient tensor η'_{ijk} given by

$$\eta'_{ijk} = \eta_{ijk} - \tfrac{1}{4}\left(\delta_{ik}\eta_{jpp} + \delta_{jk}\eta_{ipp}\right), \tag{11}$$

where δ_{ij} is the Kronecker *delta*. Fleck and Hutchinson (1997) intended to determine c_1, c_2, and c_3 from experimental data. However, Gao et al. (1999a) determined these constants from dislocation models of plane strain bending, pure torsion and two-dimensional axisymmetric void growth. Their results indicate

$$c_1 = 0, \quad c_2 = \tfrac{1}{4}, \quad c_3 = 0 \tag{12}$$

such that the effective strain gradient is

$$\eta = \sqrt{\tfrac{1}{4}\eta'_{ijk}\eta'_{ijk}}, \tag{13}$$

which, interestingly, is similar to the von Mises effective strain in conventional plasticity

$$\epsilon = \sqrt{\tfrac{2}{3}\epsilon'_{ij}\epsilon'_{ij}}, \qquad \epsilon'_{ij} = \epsilon_{ij} - \tfrac{1}{3}\delta_{ij}\epsilon_{pp}, \qquad \epsilon_{ij} = \tfrac{1}{2}\left(u_{i,j} + u_{j,i}\right). \tag{14}$$

One method of linking Taylor's model to continuum theories is the MSG plasticity (Gao et al., 1999a) which is based on a multiscale, hierarchical framework illustrated in Fig. 1(a). A mesoscale cell with linear variation of strain field is considered. Each point within the cell is considered as a microscale sub-cell within which dislocation interaction is assumed to obey the Taylor relation so that the strain gradient law of Eq. (7) applies. On the microscale, the η term is simply viewed as a measure of the density of geometrically necessary dislocations whose accumulation increases the flow stress. In other words, microscale plastic flow is assumed to occur as slip of statistically stored dislocations in a background of geometrically necessary

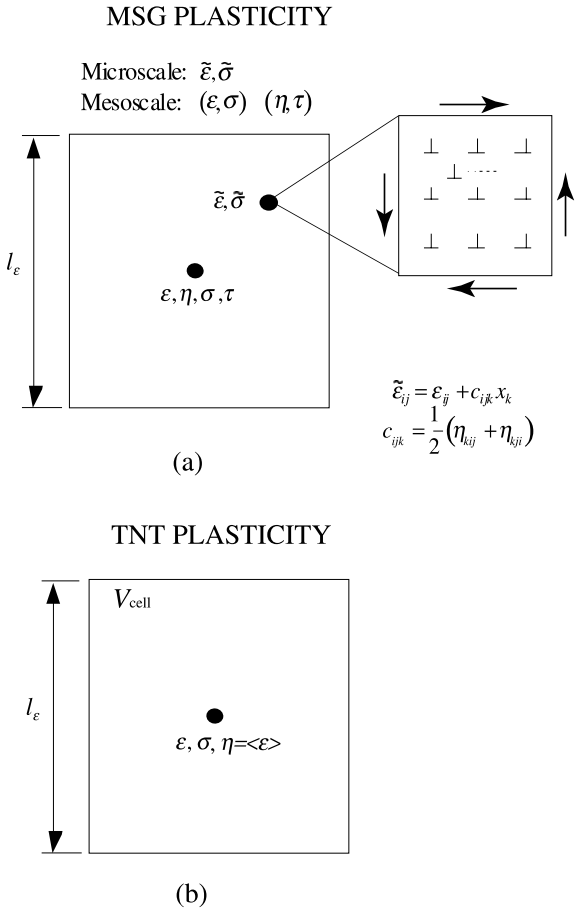

Fig. 1. (a) The multiscale framework for mechanism-based strain gradient plasticity; the microscale strains $\tilde{\epsilon}$ and stresses $\tilde{\sigma}$ are linked to dislocation interaction via the Taylor relation; strain gradients η and higher-order stresses τ are introduced as local variables on the mesoscale level. (b) The framework of TNT; the strain gradients η are expressed as a nonlocal integral average of the strain field over a small representative cell to account for the effects of geometrically necessary dislocations.

dislocations and the microscale plastic deformation is assumed to obey the Taylor work hardening relation and the associative laws of conventional plasticity. The notion of geometrically necessary dislocations is connected to the gradient of the strain field on the level of the mesoscale cell. Higher-order stresses are introduced as thermodynamic conjugates of the strain gradients at the mesoscale level on which the MSG plasticity is formulated. This hierarchical structure provides a systematic approach for constructing the mesoscale constitutive laws by averaging microscale plasticity laws over the representative cell. The constitutive equations of the MSG theory is derived based on the following principles:

1. The microscale flow stress is governed by the dislocation motion and obeys the Taylor hardening relation as exhibited by the strain gradient law of Eq. (7).
2. Strain gradient plasticity is considered a mesoscale description of dislocation activities and as such it must be derivable from the dislocation-based microscale plasticity laws.
3. The associative flow rule of plastic deformation is preserved on the microscale. This is justified by linking the microscale plastic flow to slip of statistically stored dislocations in a background of geometrically necessary dislocations. The associative rule holds if dislocation slip is assumed to be proportional to the resolved Schmid stress along an appropriate slip system (Rice, 1970, 1971).

2.2. Density of geometrically necessary dislocations as a nonlocal variable of plastic strain

The density of geometrically necessary dislocations ρ_G has been expressed in terms of the gradient of plastic strain, leading to theories of strain gradient plasticity with higher-order stresses and strains. Is it possible to express ρ_G in terms of plastic strain only, in which case no higher-order stresses need to be introduced? The answer to this question is positive if one considers the framework of nonlocal plasticity.

To see the essential idea, let us first ask the question: Why was the hierarchical framework shown in Fig. 1(a) necessary for the development of MSG theory? The reason is that the mesoscale was necessary to link the density of geometrically necessary dislocations to strain gradients which become higher-order strains in the constitutive equations. However, an alternative way of accomplishing this linkage is to write strain gradients as a nonlocal integral of strains such that ρ_G can be calculated from strains without having to resort to the mesoscale. Consider the Taylor expansion of a strain component ϵ_{ij} in the neighborhood of point $\boldsymbol{x}$

$$\epsilon_{ij}(\boldsymbol{x}+\boldsymbol{\xi}) = \epsilon_{ij}(\boldsymbol{x}) + \epsilon_{ij,m}\xi_m + \mathrm{O}(|\boldsymbol{\xi}|^2), \tag{15}$$

where $\boldsymbol{\xi}$ denotes local coordinates centered at $\boldsymbol{x}$. Integrating this equation with ξ_k over a small representative volume V_{cell} containing $\boldsymbol{x}$ (Fig. 1(b)), we find

$$\int_{V_{\mathrm{cell}}} \epsilon_{ij}(\boldsymbol{x}+\boldsymbol{\xi})\xi_k \,\mathrm{d}V = \epsilon_{ij}(\boldsymbol{x}) \int_{V_{\mathrm{cell}}} \xi_k \,\mathrm{d}V + \epsilon_{ij,m} \int_{V_{\mathrm{cell}}} \xi_k\xi_m \,\mathrm{d}V, \tag{16}$$

where the characteristic size, ℓ_ϵ, of V_{cell} is assumed to be sufficiently small such that terms of higher order in ℓ_ϵ are negligible. Therefore, the gradient term $\epsilon_{ij,k}$ can be expressed in terms of an integral of strain ϵ,

$$\epsilon_{ij,k} = \int_{V_{\mathrm{cell}}} \left[\epsilon_{ij}(\boldsymbol{x}+\boldsymbol{\xi}) - \epsilon_{ij}(\boldsymbol{x})\right]\xi_m \,\mathrm{d}V \left(\int_{V_{\mathrm{cell}}} \xi_k\xi_m \,\mathrm{d}V \right)^{-1}, \tag{17}$$

where $\left(\int_{V_{\mathrm{cell}}} \xi_k\xi_m \,\mathrm{d}V\right)^{-1}$ is the inverse of $\int_{V_{\mathrm{cell}}} \xi_k\xi_m \,\mathrm{d}V$. In the case of a cubic representative cell centered at $\boldsymbol{x}$, Eq. (17) reduces to

$$\epsilon_{ij,k} = \frac{1}{I_\epsilon} \int_{V_{\mathrm{cell}}} \epsilon_{ij}\xi_k \,\mathrm{d}V, \tag{18}$$

where I_ϵ is the moment of inertia of the representative cell and is related to the edge length ℓ_ϵ of the cube by

$$I_\epsilon = \int_{V_{\text{cell}}} \xi_1^2 \, \mathrm{d}V = \frac{1}{12}\ell_\epsilon^5. \tag{19}$$

The above example is the key idea of this paper. By representing strain gradients as a nonlocal integral of strains we will be able to calculate the density of geometrically necessary dislocations as a nonlocal variable in the constitutive equations which involves no higher-order stresses nor strain gradients. We shall adopt the following guiding principles in the nonlocal constitutive framework:

1. The flow stress obeys the Taylor hardening relation as exhibited by the strain gradient law of Eq. (7).
2. The density of geometrically necessary dislocations is calculated as nonlocal variables expressed in terms of a weighted average of plastic strain.
3. The essential structure of classical plasticity is preserved.

According to Eqs. (6) and (13), the density of geometrically necessary dislocations is related to the strain gradient tensor as $\rho_{\text{G}} = 2\eta/b$, where $\eta = \sqrt{\eta'_{ijk}\eta'_{ijk}/4}$. In the nonlocal constitutive framework to be discussed below, the deviatoric strain gradients η'_{ijk} in Eq. (11) will be treated as nonlocal variables,

$$\eta'_{ijk} = \frac{1}{I_\epsilon}\int_{V_{\text{cell}}} \left[\epsilon_{ik}\xi_j + \epsilon_{jk}\xi_i - \epsilon_{ij}\xi_k - \frac{1}{4}\left(\delta_{ik}\xi_j + \delta_{jk}\xi_i\right)\epsilon_{pp}\right]\mathrm{d}V, \tag{20}$$

where we have assumed a cubic representative cell centered at $\boldsymbol{x}$ for simplicity. In the limit of $\ell_\epsilon \to 0$, the right-hand side of Eq. (20) naturally converges to the strain gradient form of η'_{ijk}. The general averaging procedure described in Eq. (17) should be used for cells of other shapes and for points near the boundary.

2.3. Deformation theory of TNT

The deformation theory of Taylor-based nonlocal theory (TNT) of plasticity assumes the same structure as the classical plasticity theories (Hill, 1950). The strains are decomposed into a volumetric part and a deviatoric part,

$$\epsilon_{ij} = \tfrac{1}{3}\epsilon_{kk}\delta_{ij} + \epsilon'_{ij}. \tag{21}$$

The volumetric strain ϵ_{kk} is related to the hydrostatic stress σ_{kk} via the elastic bulk modulus $K = E/[3(1-2\nu)]$ (E is Young's modulus and ν, Poisson's ratio),

$$\epsilon_{kk} = \frac{\sigma_{kk}}{3K}. \tag{22}$$

The deviatoric strains ϵ'_{ij} are proportional to deviatoric stresses $\sigma'_{ij} = \sigma_{ij} - \frac{1}{3}\sigma_{kk}\delta_{ij}$ such that

$$\epsilon'_{ij} = \lambda\sigma'_{ij} \tag{23}$$

with the coefficient λ given by

$$\lambda = \left(\frac{\epsilon'_{ij}\epsilon'_{ij}}{\sigma'_{ij}\sigma'_{ij}}\right)^{1/2} = \frac{3\epsilon}{2\sigma_{\text{e}}}, \tag{24}$$

where $\epsilon = \sqrt{(2/3)\epsilon'_{ij}\epsilon'_{ij}}$ is the effective strain as in Eq. (14), and

$$\sigma_{\text{e}} = \sqrt{\tfrac{3}{2}\sigma'_{ij}\sigma'_{ij}} \tag{25}$$

is the effective stress. The yield criterion is

$$\sigma_e = \sigma = \sigma_{ref}\sqrt{f^2(\epsilon) + \ell\eta}. \tag{26}$$

Combining these relationships lead to the following constitutive equations for the deformation theory of TNT:

$$\sigma_{kk} = 3K\epsilon_{kk}, \tag{27}$$

$$\sigma'_{ij} = \frac{2\sigma_{ref}\sqrt{f^2(\epsilon) + \ell\eta}}{3\epsilon}\epsilon'_{ij}, \tag{28}$$

where $\ell = 18\alpha^2(\mu/\sigma_{ref})^2 b$ has been given in Eq. (8) and η is a nonlocal variable defined by Eqs. (13) and (20).

2.4. Flow theory of TNT

In the flow theory of TNT, the constitutive equations are expressed in rate form. The strain rates can be decomposed into a volumetric part and a deviatoric part

$$\dot{\epsilon}_{ij} = \tfrac{1}{3}\dot{\epsilon}_{kk}\delta_{ij} + \dot{\epsilon}'_{ij}, \tag{29}$$

where the volumetric strain rate is purely elastic and is related to the hydrostatic stress rate $\dot{\sigma}_{kk}$ as

$$\dot{\epsilon}_{kk} = \frac{\dot{\sigma}_{kk}}{3K}. \tag{30}$$

The deviatoric strain rate consists of an elastic part and a plastic part,

$$\dot{\epsilon}'_{ij} = \dot{\epsilon}^{e'}_{ij} + \dot{\epsilon}^{p}_{ij}, \tag{31}$$

where the elastic strain rate $\dot{\epsilon}^{e'}_{ij}$ is proportional to the deviatoric stress rate $\dot{\sigma}'_{ij}$ via the shear modulus μ,

$$\dot{\epsilon}^{e'}_{ij} = \frac{\dot{\sigma}'_{ij}}{2\mu}. \tag{32}$$

The plastic strain rate $\dot{\epsilon}^{p}_{ij}$ is proportional to the deviatoric stress $\sigma'_{ij} = \sigma_{ij} - \sigma_{kk}\delta_{ij}/3$ by the associative rule

$$\dot{\epsilon}^{p}_{ij} = \lambda\sigma'_{ij} \tag{33}$$

with the coefficient λ given by

$$\lambda = \left(\frac{\dot{\epsilon}^{p}_{ij}\dot{\epsilon}^{p}_{ij}}{\sigma'_{ij}\sigma'_{ij}}\right)^{1/2} = \frac{3\dot{\epsilon}^{p}}{2\sigma_e}, \tag{34}$$

where

$$\dot{\epsilon}^{p} = \sqrt{\tfrac{2}{3}\dot{\epsilon}^{p}_{ij}\dot{\epsilon}^{p}_{ij}} \tag{35}$$

is the effective plastic strain rate and $\sigma_e = \sqrt{3\sigma'_{ij}\sigma'_{ij}/2}$ is the effective stress. Combining Eqs. (31)–(34) leads to

$$\dot{\sigma}'_{ij} = 2\mu\left(\dot{\epsilon}'_{ij} - \frac{3\dot{\epsilon}^{p}}{2\sigma_e}\sigma'_{ij}\right). \tag{36}$$

The effective plastic strain ϵ^{p} is obtained from the effective plastic strain rate $\dot{\epsilon}^{p}$ as

$$\epsilon^{p} = \int \dot{\epsilon}^{p}\,\mathrm{d}t. \tag{37}$$

For the flow theories of plasticity, it is useful to write the uniaxial stress–strain relation in terms of the plastic strain ϵ^{p} as

$$\sigma = \sigma_{\mathrm{ref}} f_{\mathrm{p}}(\epsilon^{\mathrm{p}}), \tag{38}$$

where f_{p} is a function of plastic strain, and it is related to the elastic–plastic uniaxial stress–strain relation $\sigma = \sigma_{\mathrm{ref}} f(\epsilon)$ in previous sections by

$$f_{\mathrm{p}}(\epsilon^{\mathrm{p}}) = f(\epsilon) = f\left[\epsilon^{\mathrm{p}} + \frac{\sigma_{\mathrm{ref}}}{E} f_{\mathrm{p}}(\epsilon^{\mathrm{p}})\right]. \tag{39}$$

The yield criterion is

$$\sigma_{\mathrm{e}} = \sigma = \sigma_{\mathrm{ref}} \sqrt{f_{\mathrm{p}}^2(\epsilon^{\mathrm{p}}) + \ell\eta}. \tag{40}$$

Differentiating the square of Eq. (40) with respect to time gives the consistency condition

$$2\sigma_{\mathrm{e}}\dot{\sigma}_{\mathrm{e}} = 3\sigma'_{ij}\dot{\sigma}'_{ij} = \sigma_{\mathrm{ref}}^2\left(2f_{\mathrm{p}}f'_{\mathrm{p}}\dot{\epsilon}^{\mathrm{p}} + \ell\dot{\eta}\right), \tag{41}$$

where

$$\dot{\eta} = \frac{1}{4\eta}\eta'_{ijk}\dot{\eta}'_{ijk}, \tag{42}$$

$$\dot{\eta}'_{ijk} = \frac{1}{I_\epsilon}\int_{V_{\mathrm{cell}}}\left[\dot{\epsilon}_{ik}\xi_j + \dot{\epsilon}_{jk}\xi_i - \dot{\epsilon}_{ij}\xi_k - \frac{1}{4}\left(\delta_{ik}\xi_j + \delta_{jk}\xi_i\right)\dot{\epsilon}_{pp}\right]\mathrm{d}V \tag{43}$$

are obtained from Eqs. (13) and (20), respectively. Inserting Eq. (36) into Eq. (41) leads to

$$\dot{\epsilon}^{\mathrm{p}} = \frac{6\mu\sigma'_{ij}\dot{\epsilon}'_{ij} - \sigma_{\mathrm{ref}}^2\ell\dot{\eta}}{2(3\mu\sigma_{\mathrm{e}} + \sigma_{\mathrm{ref}}^2 f_{\mathrm{p}}f'_{\mathrm{p}})}. \tag{44}$$

Taking account of the possibility of elastic unloading, the plastic strain rate $\dot{\epsilon}^{\mathrm{p}}$ is given by

$$\dot{\epsilon}^{\mathrm{p}} = \begin{cases} \frac{6\mu\sigma'_{ij}\dot{\epsilon}'_{ij} - \sigma_{\mathrm{ref}}^2\ell\dot{\eta}}{2(3\mu\sigma_{\mathrm{e}} + \sigma_{\mathrm{ref}}^2 f_{\mathrm{p}}f'_{\mathrm{p}})} & \text{if } \sigma_{\mathrm{e}} = \sigma \quad \text{and} \quad \dot{\sigma}_{\mathrm{e}} \geqslant 0, \\ 0 & \text{if } \sigma_{\mathrm{e}} < \sigma \quad \text{or} \quad \dot{\sigma}_{\mathrm{e}} < 0. \end{cases} \tag{45}$$

Finally, the constitutive equations for the flow theory of TNT plasticity are assembled as

$$\dot{\sigma}_{kk} = 3K\dot{\epsilon}_{kk}, \tag{46}$$

$$\dot{\sigma}'_{ij} = \begin{cases} 2\mu\left(\dot{\epsilon}'_{ij} - \frac{3\sigma'_{ij}}{4\sigma}\frac{6\mu\sigma'_{kl}\dot{\epsilon}'_{kl} - \sigma_{\mathrm{ref}}^2\ell\dot{\eta}}{3\mu\sigma_{\mathrm{e}} + \sigma_{\mathrm{ref}}^2 f_{\mathrm{p}}f'_{\mathrm{p}}}\right) & \text{if } \sigma_{\mathrm{e}} = \sigma \quad \text{and} \quad \dot{\sigma}_{\mathrm{e}} \geqslant 0, \\ 2\mu\dot{\epsilon}'_{ij} & \text{if } \sigma_{\mathrm{e}} < \sigma \quad \text{or} \quad \dot{\sigma}_{\mathrm{e}} < 0, \end{cases} \tag{47}$$

where the nonlocal variable $\dot{\eta}$ is given by the strain rates according to Eqs. (42) and (43).

Under proportional deformation, it can be shown that the flow theory of TNT coincides with the deformation theory of TNT.

It is interesting at this point to make a comparison between TNT and the classical plasticity. In the classical flow theory, the consistency condition is used to derive a point-wise relation between the stress rate and strain rate,

$$\dot{\boldsymbol{\sigma}} = \boldsymbol{D}^{\mathrm{ep}}(\boldsymbol{\sigma}) : \dot{\boldsymbol{\epsilon}}, \tag{48}$$

where $\boldsymbol{D}^{\mathrm{ep}}(\boldsymbol{\sigma})$ is the local elastic–plastic stiffness tensor. In contrast, the TNT flow theory has a nonlocal relation between the stress rates and strain rates,

$$\dot{\boldsymbol{\sigma}} = \boldsymbol{G}(\boldsymbol{\epsilon}, \dot{\boldsymbol{\epsilon}}, \langle \boldsymbol{\epsilon} \rangle, \langle \dot{\boldsymbol{\epsilon}} \rangle), \tag{49}$$

where $\langle \ldots \rangle$ denotes integral average over a small representative volume.

In the strain-based algorithm of TNT, the stress rate is fully determined from the current strain field and a kinematically admissible strain rate. However, in a stress-based algorithm, an integral equation needs to be solved for strain rates in terms of the given stress rates. Also, we note that the representative volume in TNT is only used to determine the gradients of the strain field. The size of the averaging cell is thus not a material constant and should be made sufficiently small as well as convenient in practical numerical implementations.

2.5. Balance laws

The balance laws of a nonlocal continuum theory are identical to those of the classical local theories (Eringen, 1981, 1983). This is also the case for TNT plasticity. For example, the balance of angular and linear momentum leads to a symmetric stress tensor σ_{ij} which satisfies the equilibrium equation

$$\sigma_{ij,i} + f_j = \rho \dot{v}_j, \tag{50}$$

where f_j denotes the body force, ρ the mass density and v_j the velocity.

2.6. Intrinsic length in TNT

As discussed before, the size of the averaging cell should not be regarded as a material constant; it should be made sufficiently small as well as convenient in practical numerical implementations. The strain gradient length ℓ in Eq. (8), however, is an intrinsic material length that represents a combined effect of elasticity (shear modulus μ), plasticity (reference stress σ_{ref} in uniaxial tension), and the atomic nature of solids (Burgers vector b). The intrinsic material length ℓ has been modified (Huang et al., 1999, 2000b) from its original expression (Nix and Gao, 1998) in order to account for the effect of crystallinity of materials (e.g., Taylor's factor, Nye's factor). The preliminary results based on the TNT plasticity with the intrinsic material length in Eq. (8) agree well with microscale experiments (see Section 4 for details).

We would like to point out that, although the intrinsic material length ℓ in Eq. (8) appears to depend on how the reference stress σ_{ref} is defined, the TNT theory is independent of the choice of σ_{ref}. This can be seen from the flow stress in Eq. (26), which can be written as

$$\sigma = \sqrt{[\sigma_{\mathrm{ref}} f(\epsilon)]^2 + 18(\alpha\mu)^2 b\eta} \tag{51}$$

which depends only on the uniaxial stress–strain relation and the effective strain gradient, but not on the precise definition of σ_{ref}. In other words, even though σ_{ref} and ℓ appear in the formulation of TNT plasticity, they always appear in the form of $\sigma_{\mathrm{ref}} f(\epsilon)$ or $\sigma_{\mathrm{ref}}^2 \ell$ such that TNT plasticity is independent of σ_{ref}.

Only for the purpose of estimating the intrinsic material length ℓ will one need to define the reference stress σ_{ref} in uniaxial tension. A convenient choice is through the power-law stress–strain relation, $\sigma = \sigma_{\mathrm{ref}} \epsilon^N$ (N is the plastic work hardening exponent). The intrinsic material length in Eq. (8) is approximately 4 μm for copper with the parameters $\alpha = 1$, $b = 0.255$ nm, $\mu = 0.375E$ (E is Young's modulus), $\sigma_{\mathrm{ref}} = E\epsilon_{\mathrm{Y}}^{1-N}$, $\epsilon_{\mathrm{Y}} = 0.002$ is the yield strain, and $N = 0.3$ is the plastic work hardening exponent. This agrees with the estimate of Fleck et al. (1994) from micro-torsion experiments.

3. Applications

We use TNT plasticity to investigate several phenomena that are related to plasticity at the micron scale in this section. For simplicity, we neglect the elastic deformation such that the material is incompressible. Accordingly, the deviatoric strain gradient tensor η'_{ijk} becomes the same as the strain gradient tensor η_{ijk}.

3.1. Bending of thin beams

Consider bending of ultra-thin beams under plane-strain conditions. The Cartesian reference frame is set such that the x_1 axis coincides with the neutral axis of the beam, and bending is applied in the (x_1, x_2) plane. A unit beam width is taken in the out-of-plane (x_3) direction. The curvature is designated κ and the beam thickness is designated h. Strains in the Cartesian reference frame are given by

$$\epsilon_{11} = -\epsilon_{22} = \kappa x_2, \qquad \epsilon_{12} = 0, \tag{52}$$

where ϵ_{22} is obtained from the assumptions of plane strain deformation ($\epsilon_{33} = 0$) and incompressibility ($\epsilon_{kk} = 0$). The nonlocal strain gradients are calculated according to Eq. (20), by an integral average of the strain field over the representative volume. For example

$$\eta_{112} = \frac{1}{I_\epsilon}\int_{V_{\text{cell}}} (-\epsilon_{11}\xi_2)\,\mathrm{d}V = \frac{1}{I_\epsilon}\int_{V_{\text{cell}}} [-\kappa(x_2+\xi_2)\xi_2]\,\mathrm{d}V = -\kappa. \tag{53}$$

Similar calculations give all the nonzero components of strain gradients as

$$\eta_{112} = \eta_{222} = -\kappa, \qquad \eta_{121} = \eta_{211} = \kappa. \tag{54}$$

The effective strain ϵ and effective strain gradient η are given by

$$\epsilon = \frac{2}{\sqrt{3}}\kappa|x_2|, \qquad \eta = \kappa. \tag{55}$$

The monotonically increasing bending curvature κ results in proportional deformation under which the flow theory of TNT coincides with the deformation theory. The constitutive equation (28) give nonvanishing deviatoric stresses as

$$\sigma'_{11} = -\sigma'_{22} = \operatorname{sign}(x_2)\frac{\sigma}{\sqrt{3}}, \tag{56}$$

where $\operatorname{sign}(x_2)$ stands for the sign of x_2 and σ is the flow stress given in Eq. (26).

The equilibrium equation (50) and traction-free boundary conditions on the top and bottom surfaces of the beam ($x_2 = \pm h/2$) give the hydrostatic stress

$$\sigma_{kk} = -3\sigma'_{22}. \tag{57}$$

The traction at the cross-section of the beam is

$$\sigma_{11} = \sigma'_{11} + \frac{1}{3}\sigma_{kk} = \operatorname{sign}(x_2)\frac{2\sigma}{\sqrt{3}} \tag{58}$$

which gives a pure bending moment M as

$$M = \int_{-h/2}^{h/2} \frac{2}{\sqrt{3}}|x_2|\sigma\,\mathrm{d}x_2. \tag{59}$$

This moment–curvature relation differs from the corresponding result for MSG plasticity derived by Huang et al. (2000a) by a term of order ℓ_ϵ^2 which is negligibly small. The difference between TNT and MSG

plasticity theories results from the higher-order stresses, which exist only in MSG plasticity and are on the order of ℓ_ϵ^2. Huang et al. (2000a) already pointed out that the moment–curvature relation is insensitive to ℓ_ϵ^2.

3.2. Torsion of thin wires

We apply TNT plasticity to investigating torsion of thin wires. The Cartesian reference frame is set such that the x_1 and x_2 axes are within the cross-section of the wire, while the x_3 axis coincides with the central axis of the wire. The twist per unit length is designated κ and the radius of the wire is designated a. The nonvanishing strains in the Cartesian reference frame are

$$\epsilon_{13} = \epsilon_{31} = -\frac{\kappa}{2}x_2, \qquad \epsilon_{23} = \epsilon_{32} = \frac{\kappa}{2}x_1. \tag{60}$$

The nonlocal strain gradients are calculated by integral average of the strain field as in Eq. (20). For example,

$$\eta_{231} = \frac{1}{I_\epsilon}\int_{V_{\text{cell}}} (\epsilon_{13}\xi_2 - \epsilon_{23}\xi_1)\,\mathrm{d}V = -\kappa. \tag{61}$$

Similar calculations lead to the rest of the nonlocal strain gradients

$$\eta_{231} = \eta_{321} = -\kappa, \qquad \eta_{132} = \eta_{312} = \kappa. \tag{62}$$

The effective strain ϵ and effective strain gradient η are given by

$$\epsilon = \frac{1}{\sqrt{3}}\kappa r, \quad \eta = \kappa, \tag{63}$$

where $r = \sqrt{x_1^2 + x_2^2}$ is the radius in polar coordinates (r, θ).

The monotonically increasing twist κ results in proportional deformation under which condition the flow theory coincides with the deformation theory. The constitutive equation (28) give nonvanishing deviatoric stresses as

$$\sigma'_{13} = \sigma'_{31} = -\frac{\sin\theta}{\sqrt{3}}\sigma, \qquad \sigma'_{23} = \sigma'_{32} = \frac{\cos\theta}{\sqrt{3}}\sigma, \tag{64}$$

where σ is the flow stress given in Eq. (26), and θ, the polar angle in polar coordinates.

The equilibrium equation (50) and traction-free boundary conditions on the lateral surface of the wire ($r = a$) give a vanishing hydrostatic stress, i.e.,

$$\sigma_{kk} = 0. \tag{65}$$

The shear stresses in the cross section of the wire σ'_{31} and σ'_{32} correspond to a pure torque T which is found from integration

$$T = \frac{2}{\sqrt{3}}\pi\int_0^a \sigma r^2\,\mathrm{d}r. \tag{66}$$

This torque versus twist-per-unit-length relation differs from the corresponding equation for MSG plasticity derived by Huang et al. (2000a) by a negligible term of order ℓ_ϵ^2.

3.3. Growth of microvoids

The nucleation, growth and coalescence of microvoids is a common fracture mechanism of ductile metals. Although there have been significant studies on the mechanics of void growth based on classical plasticity theory (e.g., Rice and Tracy, 1969; Gurson, 1977; Tvergaard, 1990; Huang, 1991; Needleman

et al., 1992), these studies do not show any dependence on void size since classical plasticity theories do not involve an intrinsic material length. It is therefore of interest to investigate the effect of void size on the void growth phenomena, particularly for micron- and submicron-sized voids. In this section, we use TNT plasticity to investigate the growth of a spherical void in an infinite medium subjected to remote spherically symmetric tension.

A spherical void of initial radius R_0 in an infinite medium is subjected to remote spherically symmetric tension, σ^∞. The spherical coordinates (R, θ, ϕ) are used. The solid is incompressible, so that the nonvanishing displacement in spherical coordinates is

$$u_R = \frac{R_0^2}{R^2} u_0, \tag{67}$$

where u_0 is the displacement on the void surface. The nonvanishing strains in spherical coordinates are

$$\epsilon_{RR} = -2\epsilon_{\theta\theta} = -2\epsilon_{\phi\phi} = -2\frac{R_0^2}{R^3} u_0. \tag{68}$$

The nonlocal strain gradients are calculated by the integral averaging formula given in Eq. (20). For example,

$$\eta_{RRR} = \frac{1}{I_\epsilon} \int_{V_{\text{cell}}} \epsilon_{RR} \xi_R \, \mathrm{d}V = \frac{6R_0^2}{R^4} u_0, \tag{69}$$

where terms of order ℓ_ϵ^2 are neglected. By similar calculations one can find all the nonzero components of the nonlocal strain gradients,

$$\eta_{RRR} = -2\eta_{R\theta\theta} = -2\eta_{\theta R\theta} = -2\eta_{R\phi\phi} = -2\eta_{\phi R\phi} = -2\eta_{\theta\theta R} = -2\eta_{\phi\phi R} = 6\frac{R_0^2}{R^4} u_0. \tag{70}$$

The effective strain ϵ and effective strain gradient η are given by

$$\epsilon = 2\frac{R_0^2}{R^3} u_0, \qquad \eta = 3\sqrt{\frac{5}{2}}\frac{R_0^2}{R^4} u_0. \tag{71}$$

The monotonically increasing remote stress σ^∞ causes the displacement u_0 at the void surface to increase. The deformation in the process is proportional such that the flow theory of TNT coincides with the deformation theory, and the constitutive equation (28) give nonvanishing deviatoric stresses as

$$\sigma'_{RR} = -2\sigma'_{\theta\theta} = -2\sigma'_{\phi\phi} = -\tfrac{2}{3}\sigma, \tag{72}$$

where σ is the flow stress given in Eq. (26).

The equilibrium equation (50) and traction-free boundary conditions on the void surface ($R = R_0$) give the hydrostatic stress as

$$\sigma_{kk} = -3\sigma'_{RR} - 6\int_{R_0}^{R} \frac{\sigma'_{RR} - \sigma'_{\theta\theta}}{R} \, \mathrm{d}R. \tag{73}$$

As R approaches infinity, all deviatoric stresses vanish, such that Eqs. (72) and (73) lead to the remotely applied spherically symmetric stress,

$$\sigma^\infty = 2\int_{R_0}^{\infty} \frac{\sigma}{R} \, \mathrm{d}R. \tag{74}$$

This equation differs from the corresponding MSG expression (Huang et al., 2000a) by a negligible term of order ℓ_ϵ^2.

3.4. Cavitation instabilities

A void in an elastic–plastic solid will grow unstably at sufficiently high mean stresses, a phenomenon called cavitation instability (Bishop et al., 1945; Huang et al., 1991). Fleck and Hutchinson (1997) and Huang et al. (2000a) have investigated the effect of void size on cavitation instability by the strain gradient plasticity theories. In this section, we investigate cavitation instability using the TNT theory.

A spherical void in an infinite, incompressible solid is subjected to remote spherical symmetric tension σ^{∞}. The spherical coordinates (R, θ, ϕ) in the initial configuration and (r, θ, ϕ) in the current configuration are used, where we use R to designate the initial radius of a material point in the undeformed configuration, and r to denote the current radius of the same material point in the deformed configuration. The void radius is denoted by R_0 and r_0 in the initial and current configurations, respectively. It is important to distinguish between these two configurations because finite strain effects play a crucial role in cavitation instability.

Cavitation is driven by the elastic energy stored in the remote field (Huang et al., 1991); therefore, it is essential to include elasticity in the constitutive model. We use the following elastic-power-law-hardening uniaxial stress–strain relation,

$$\sigma_{\mathrm{ref}} f(\epsilon) = \begin{cases} E\epsilon & \text{if } \epsilon \leqslant \epsilon_{\mathrm{Y}}, \\ \sigma_{\mathrm{ref}} \epsilon^{N} & \text{if } \epsilon > \epsilon_{\mathrm{Y}}, \end{cases} \tag{75}$$

where E is Young's modulus, N, the plastic work hardening exponent ($0 \leqslant N < 1$), and ϵ_{Y}, the yield strain and is related to the reference stress by $\sigma_{\mathrm{ref}} = E\epsilon_{\mathrm{Y}}^{1-N}$.

The incompressibility of the solid requires

$$R^3 - R_0^3 = r^3 - r_0^3. \tag{76}$$

Its derivative with respect to time gives the particle velocity in the current configuration,

$$v_r = \dot{r} = \frac{r_0^2}{r^2}\dot{r}_0, \tag{77}$$

where $\dot{r}_0$ is the velocity of the void surface. The strain rates in the current configuration are

$$\dot{\epsilon}_{rr} = \frac{\mathrm{d}v_r}{\mathrm{d}r}, \qquad \dot{\epsilon}_{\theta\theta} = \dot{\epsilon}_{\phi\phi} = \frac{v_r}{r}. \tag{78}$$

Because the velocity field is irrotational, we may integrate the strain rate tensor with respect to time to obtain strains in finite deformation as

$$\epsilon_{rr} = -2\ln\frac{r}{R}, \qquad \epsilon_{\theta\theta} = \epsilon_{\phi\phi} = \ln\frac{r}{R}. \tag{79}$$

The nonlocal rates of strain gradients in the current configuration are calculated by the integral averaging formula given in Eq. (20). For example

$$\dot{\eta}_{rrr} = \frac{1}{I_\epsilon}\int_{V_{\mathrm{cell}}} \dot{\epsilon}_{rr}\xi_r \mathrm{d}V = \frac{6r_0^2}{r^4}\dot{r}_0, \tag{80}$$

where terms of order ℓ_ϵ^2 are neglected. By similar calculations one can find all the nonzero components of the nonlocal rates of strain gradients

$$\dot{\eta}_{rrr} = -2\dot{\eta}_{r\theta\theta} = -2\dot{\eta}_{\theta r\theta} = -2\dot{\eta}_{r\phi\phi} = -2\dot{\eta}_{\phi r\phi} = -2\dot{\eta}_{\theta\theta r} = -2\dot{\eta}_{\phi\phi r} = \frac{6r_0^2}{r^4}\dot{r}_0. \tag{81}$$

Their integration with respect to time gives strain gradients in finite deformation,

$$\eta_{rrr} = -2\eta_{r\theta\theta} = -2\eta_{\theta r\theta} = -2\eta_{r\phi\phi} = -2\eta_{\phi r\phi} = -2\eta_{\theta\theta r} = -2\eta_{\phi\phi r} = 6\left(\frac{1}{R} - \frac{1}{r}\right). \tag{82}$$

The effective strain ϵ and effective strain gradient η are given by

$$\begin{aligned} \epsilon &= 2\ln\left(\frac{r}{R}\right) = \frac{2}{3}\ln\left(\frac{r^3}{r^3 - r_0^3 + R_0^3}\right), \\ \eta &= 3\sqrt{\frac{5}{2}}\left(\frac{1}{R} - \frac{1}{r}\right) = 3\sqrt{\frac{5}{2}}\left[\frac{1}{(r^3 - r_0^3 + R_0^3)^{1/3}} - \frac{1}{r}\right], \end{aligned} \tag{83}$$

where the radius R of the material point in the initial, undeformed configuration has been eliminated by Eq. (76).

The constitutive equation (28) give nonvanishing deviatoric true stresses in the current configuration

$$\sigma'_{rr} = -2\sigma'_{\theta\theta} = -2\sigma'_{\phi\phi} = -\tfrac{2}{3}\sigma, \tag{84}$$

where σ is the flow stress given in Eq. (26).

The equilibrium equation (50) and traction-free boundary conditions on the void surface ($r = r_0$) give the hydrostatic stress as

$$\sigma_{kk} = -3\sigma'_{rr} - 6\int_{r_0}^{r} \frac{\sigma'_{rr} - \sigma'_{\theta\theta}}{r}\,\mathrm{d}r. \tag{85}$$

As r approaches infinity, all deviatoric stresses vanish, such that Eqs. (84) and (85) lead to the remotely applied spherically symmetric stress,

$$\sigma^{\infty} = 2\int_{r_0}^{\infty} \frac{\sigma}{r}\,\mathrm{d}r. \tag{86}$$

This relation between the void radius, r_0, in the current configuration and the remotely applied stress, σ^{∞}, again differs from the MSG result of Huang et al. (2000a) by a negligible term of order ℓ_{ϵ}^2. The numerical integration of Eq. (86) has shown that, for each plastic work hardening exponent N, there always exists a maximum value for the remotely applied stress σ^{∞}. This maximum value of remotely applied stress, which typically occurs when the void radius r_0 reaches 1.3–3 times the initial void radius R_0, is called the cavitation stress and is designated σ_c; it represents the intrinsic limit for mean stress in a material.

3.5. Particle-reinforced composite

Lloyd (1994) studied an aluminum matrix reinforced by silicon carbide particles and observed increases in strength as the particle diameter was reduced from 16 to 7.5 μm with the particle volume fraction fixed at 15%. Classical plasticity cannot explain this size dependence because its constitutive model does not possess an internal material length. In this section, we use TNT plasticity to model the size dependence of composite. A rather simple model mimicking Lloyd's (1994) experiments is developed, in which several approximations are made in order to obtain an analytical solution.

The model consists of a spherical particle of radius a embedded in a concentric spherical matrix layer with an outer radius a_{m}. The ratio of radii represents the particle volume fraction c in the composite,

$$\frac{a^3}{a_{\mathrm{m}}^3} = c. \tag{87}$$

The particle is elastic, while the matrix is modeled as an elastic–plastic incompressible solid. The system is subjected to spherical symmetric tension, σ_0, on the outer surface.

Strains inside the particle are hydrostatic, $\epsilon_{ij} = \epsilon_{\rm p}\delta_{ij}$. The displacement continuity across the particle/matrix interface gives

$$u_R(R = a) = \epsilon_{\rm p} a, \tag{88}$$

where u_R is the displacement in the radial direction. Similar to void growth in Section 3.3, the incompressibility of the matrix material gives the displacements, strains and nonlocal strain gradients the same as Eqs. (67)–(70), except that the displacement u_0 is now replaced by $\epsilon_{\rm p} a$. In particular, the strains on the outer surface ($R = a_{\rm m}$) are

$$\epsilon_{RR} = -2\epsilon_{\theta\theta} = -2\epsilon_{\phi\phi} = -2\epsilon_{\rm p} c, \qquad \epsilon = 2\epsilon_{\rm p} c \quad \text{at } R = a_{\rm m}, \tag{89}$$

where c is the particle volume fraction in Eq. (87), and ϵ, the effective strain. It is observed, for an incompressible solid, the spherical symmetric strains are identical to those in uniaxial compression,

$$(\epsilon_{RR}, \epsilon_{\theta\theta}, \epsilon_{\phi\phi}) = -2\epsilon_{\rm p} c\left(1, -\tfrac{1}{2}, -\tfrac{1}{2}\right), \tag{90}$$

where $-2\epsilon_{\rm p} c$ is the (compressive) "uniaxial strain" on the outer surface, which is consistent with $\epsilon(= 2\epsilon_{\rm p} c)$ being the uniaxial tensile strain.

The flow stress and deviatoric stresses can be found from Eqs. (26) and (72), respectively. On the outer surface ($R = a_{\rm m}$), they are given by

$$\sigma = \sigma_{\rm ref}\sqrt{f^2(2\epsilon_{\rm p} c) + 3\sqrt{\frac{5}{2}}\epsilon_{\rm p}\frac{\ell}{a}c^{4/3}} \quad \text{at } R = a_{\rm m}, \tag{91}$$

$$\sigma'_{RR} = -2\sigma'_{\theta\theta} = -2\sigma'_{\phi\phi} = -\tfrac{2}{3}\sigma \quad \text{at } R = a_{\rm m}. \tag{92}$$

It should be pointed out that the spherical symmetric stresses can be decomposed into a hydrostatic part and a uniaxial part,

$$(\sigma_{RR}, \sigma_{\theta\theta}, \sigma_{\phi\phi}) = (\sigma_{\theta\theta}, \sigma_{\theta\theta}, \sigma_{\theta\theta}) + (\sigma_{RR} - \sigma_{\theta\theta}, 0, 0), \tag{93}$$

where the "uniaxial stress" $\sigma_{RR} - \sigma_{\theta\theta}$ is the same as the effective stress σ, as seen from Eq. (92). The hydrostatic part $(\sigma_{\theta\theta}, \sigma_{\theta\theta}, \sigma_{\theta\theta})$ does not cause plastic deformation.

The applied stress, σ_0, at the outer surface can be determined from the equilibrium equation (50) and continuity condition of stress tractions across the particle/matrix interface. The applied stress is then related to the strain $\epsilon_{\rm p}$ in the particle via the elastic properties of the particle as well as the plastic properties of the matrix. In order to mimic Lloyd's (1994) uniaxial tension experiments, however, we focus on the "uniaxial stress" (or effective stress) σ and the "uniaxial strain" (or effective strain) ϵ on the outer surface. From Eqs. (89) and (91), we have

$$\sigma = \sigma_{\rm ref}\sqrt{f^2(\epsilon) + \frac{3}{2}\sqrt{\frac{5}{2}}\frac{\ell}{a}c^{1/3}}\epsilon = \sqrt{\left[\sigma_{\rm ref} f(\epsilon)\right]^2 + 27\sqrt{\frac{5}{2}}\alpha^2\mu^2\frac{b}{a}c^{1/3}}\epsilon. \tag{94}$$

We have fitted the uniaxial stress–strain relation of aluminum from Lloyd's (1994) experiments by a power-law, $\sigma_{\rm ref} f(\epsilon) = 461\epsilon^{0.133}$ MPa, which is an excellent representation for the entire range of strain reported in experiments. Other material parameters are also taken from Lloyd's (1994) experiments as shear modulus $\mu = 28.5$ GPa, particle volume fraction $c = 15\%$, particle diameter $2a = 7.5$ and 16 μm. The Burgers vector of aluminum is $b = 0.286$ nm, while the coefficient in Taylor's model is $\alpha = 0.7$. For these material properties, the relation between the effective stress σ and the effective strain ϵ in Eq. (94) is shown in Fig. 2. The curve at the bottom is the uniaxial stress–strain curve for aluminum without SiC reinforcements, i.e., the power-law relation $\sigma = 461\epsilon^{0.133}$ MPa fitted from Lloyd's (1994) experiments. The other two curves in Fig. 2 correspond to particle diameter = 7.5 and 16 μm, respectively. These two curves clearly predict the size

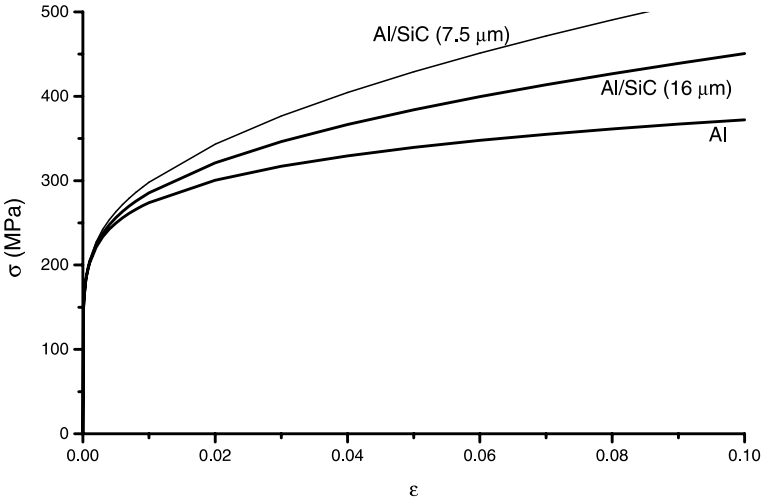

Fig. 2. The effective stress σ versus the effective strain ϵ for an Al matrix reinforced by SiC particles. The curve at the bottom is Lloyd's (1994) experimental stress–strain curve for aluminum (without SiC reinforcements), $\sigma = 461\epsilon^{0.133}$ MPa. The other two curves correspond to particle diameter = 7.5 and 16 μm, respectively.

effect observed in experiments: the smaller the particles are, the harder the material become. Moreover, the two predicted curves based on TNT plasticity agree well with the corresponding experimental curves reported by Lloyd (1994), even though the present spherically symmetric model may be overly simplistic.

4. Comparison with experiments

4.1. Micro-indentation test

Finite element method has been developed for the theory of TNT plasticity. This method will be detailed in a forthcoming paper. The indentation hardness has been calculated by the numerical method and compared with the experimental data given in Nix and Gao (1998) for polycrystalline and single crystal copper. The finite element analysis has confirmed that there are only negligible differences between TNT and MSG theories in prediction of experimentally measurable quantities.

When the depth of indentation, h, is significantly larger than 10's of microns, the strain gradients effects become negligible and the corresponding hardness degenerates to the hardness H_0 in classical plasticity. The plastic work hardening exponent is determined as $N = 0.3$ from the uniaxial stress–strain data for copper documented by McLean (1962), which is consistent with the experiments of Fleck et al. (1994) for polycrystal copper. The reference stress in uniaxial tension is $\sigma_{\text{ref}} = 408$ MPa. This leads to a prediction of the indentation hardness $H_0 = 834$ MPa for a large depth of indentation ($\gg$microns), which agrees with the experimentally measured hardness for polycrystal copper discussed by Nix and Gao (1998).

The Burgers vector for copper is $b = 0.255$ nm. The empirical constant α in the Taylor model, which should be on the order of 1 (Nix and Gibeling, 1985), is determined to be 0.7 by fitting micro-indentation hardness data for polycrystal copper. Fig. 3 presents the theoretically predicted micro-indentation hardness $(H/H_0)^2$, versus the inverse of indentation depth, $1/h$, where H is the micro-indentation hardness, H_0, the indentation hardness without the strain gradient effects, and h, the depth of indentation. The experimental data of McElhaney et al. (1998), as replotted by Nix and Gao (1998), are shown in Fig. 3 for comparison.

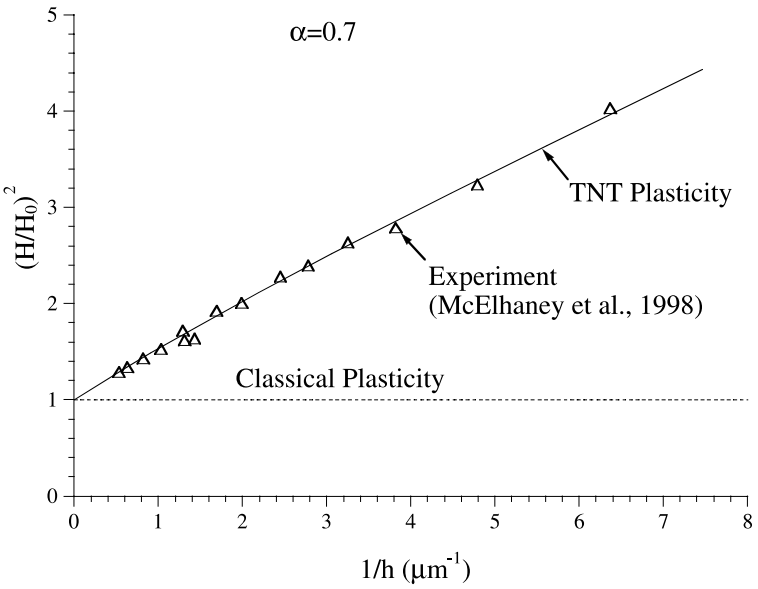

Fig. 3. Depth dependence of the hardness of polycrystal copper. The solid line is the theoretically predicted hardness. The triangles are experimental data from McElhaney et al. (1998); H is the micro-indentation hardness, H_0, the indentation hardness without strain gradient effects (i.e., for large depth of indentation), h, the depth of indentation.

It is clearly observed that the predicted hardness agrees well with the experimentally measured micro-indentation hardness data over a wide range of indentation depth, from one tenth of a micron to several microns. The parameter α estimated from the experimental data has the correct order of magnitude. Moreover, the numerical results based on TNT plasticity do give a straight line in Fig. 3, consistent with the estimate based on dislocation models (Nix and Gao, 1998).

4.2. Micro-torsion test

Fig. 4 compares the predictions from TNT plasticity with the micro-torsion experiment of Fleck et al. (1994). The uniaxial stress–strain relation $\sigma = \sigma_{\text{ref}} f(\epsilon)$ used in the analysis is taken from the micro-tension data also reported by these authors. The only adjustable parameter in TNT theory is the empirical coefficient α which is on the order of 1 from macroscopic experimental observations (e.g., Nix and Gibeling, 1985). If α is taken to be 1, we find a maximum of 14% discrepancy between the theory and experiment. This discrepancy may be attributed to extraordinarily large plastic strain involved in the wire twisting experiment of Fleck et al. (1994), which reaches as large as 120% on the wire surface. At such a strain level, there are currently no reliable data on uniaxial stress–strain behavior. (The maximum strain reported in Fleck et al.'s uniaxial tension experiment is around 10%.) Moreover, the analysis in Section 3.2 is limited to infinitesimal deformation, while very large strain occurred in the experiments of Fleck et al. (1994). In view of these considerations, the comparison in the torsion case is not unreasonable.

4.3. Micro-bending test

Fig. 5 compares the predictions of TNT with the micro-bending test of thin Ni beams by Stolken and Evans (1998). The uniaxial stress–strain relation $\sigma = \sigma_{\text{ref}} f(\epsilon)$ used in the analysis is taken from their micro-

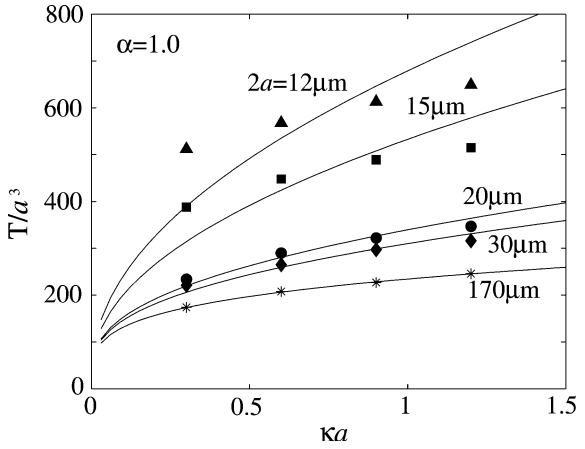

Fig. 4. Comparison of the TNT theory with the micro-torsion test of Fleck et al. (1994). Solid lines are the theoretical predictions; a is the wire radius; T, the torque; κ, the twist per unit length.

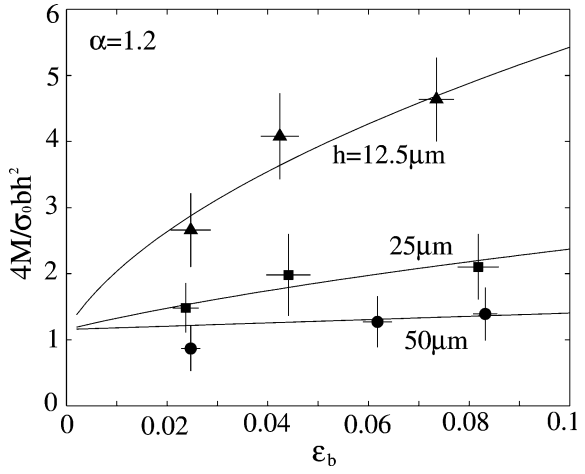

Fig. 5. Comparison of the TNT theory with the micro-bending test of Stolken and Evans (1998). Solid lines are the theoretical predictions; h is the beam thickness; b, the beam width; M, the bending moment; σ_0, the initial yield stress; ϵ_b, the maximum strain on the surface.

tension data. The empirical coefficient α is taken to be 1.2. Excellent agreement is found between theory and experiment.

5. Discussion

The TNT theory proposed in this paper follows the same guiding principles as our previously proposed MSG theory. Both TNT and MSG are aimed to model size dependent plasticity over a scale from a fraction of a micron to 10's of microns. Both theories are established on the foundation of Taylor's model of

dislocation hardening. We have shown that TNT and MSG give identical predictions for micro-bending, micro-torsion, void growth, cavitation instability, and micro-indentation. The two theories differ in their basic theoretical framework. In MSG, the density of geometrically necessary dislocations is treated as a higher-order local variable. In TNT, the density of geometrically necessary dislocations is treated as a nonlocal variable expressed in terms of an integral average of plastic strain.

The trade-off between MSG and TNT is clear. The MSG is a higher-order but local theory where both strain and strain gradients are treated as local variables. The advantage of MSG is its constitutive formulation remaining local such that stresses and higher-order stresses are related pointwise to strains and higher-order strains. In contrast, the advantage of TNT is the simplicity of its governing equations and constitutive laws all remaining "classical" in that no higher-order stresses and strains are involved.

The integral average in Eq. (18) is in fact identical to a finite difference representation of a derivative. For example, in the one-dimensional case, Eqs. (18) and (19) reduce to

$$\frac{\partial \epsilon}{\partial x} = \frac{1}{I_\epsilon} \int_{-\ell_\epsilon/2}^{\ell_\epsilon/2} \epsilon(x+\xi)\xi \, \mathrm{d}\xi, \tag{95}$$

where

$$I_\epsilon = \int_{-\ell_\epsilon/2}^{\ell_\epsilon/2} \xi^2 \mathrm{d}\xi = \frac{\ell_\epsilon^3}{12}. \tag{96}$$

Using the two-point integration rule of Gaussian quadrature in evaluating the integral of Eq. (95), we obtain

$$\frac{\partial \epsilon}{\partial x} = \frac{\epsilon(x+\Delta\xi) - \epsilon(x-\Delta\xi)}{2\Delta\xi}, \tag{97}$$

where

$$\Delta\xi = \frac{\ell_\epsilon}{2\sqrt{3}}. \tag{98}$$

It is clear from this example that the cell size ℓ_ϵ of TNT is analogous to the step size in the finite difference representation of a derivative.

We can also compare TNT and MSG theories from a partial-differential-equations (PDE) point of view. The govern equations in classical continuum mechanics are second order PDEs for displacements. The Nix–Gao strain gradient law of Eq. (7) introduces a first order gradient in the constitutive equations of continuum mechanics, leading to a third order PDE. However, an odd-ordered PDE in continuum mechanics is always ill posed because one needs to apply the same number of boundary conditions on each boundary. This can be clearly seen from a one-dimensional problem with boundary conditions given at the two ends. A third order PDE would require unequal number of boundary conditions at the ends. This problem is resolved very differently in TNT and MSG. In MSG plasticity, we augment the third order PDE to fourth order by introducing the work conjugate of strain gradients (i.e. the higher-order stresses) on the mesoscale level. The governing PDE in MSG are thus of fourth order, and additional boundary conditions come from the higher-order stress tractions. In TNT plasticity, we reduce the third order PDE back to second order by writing the strain gradients as a nonlocal integral average of strains, which is equivalent to a finite difference representation of strain gradients in terms of strain values in the neighborhood of a material point. In some sense, what we are trying to do is to evenize the order of PDE's in continuum mechanics. From this point of view, it is clear that the cell size ℓ_ϵ of TNT cannot be zero because in that limit the order of PDE increases by 1. The finite step size is necessary to keep the order of differential

equations from increasing; at the same time it should also be taken as small as possible in practical calculations for accurate estimate of the strain gradients.

6. Summary

In this paper, the following objectives have been achieved:

(1) We have proposed a TNT non local theory of plasticity to model size-dependent plasticity at the micron scale. This theory falls within the essential structure of classical plasticity theories except that the effect of geometrically necessary dislocations is introduced in the constitutive framework as a nonlocal variable measuring the curvature of plastic deformation in a representative volume. The TNT theory conforms to the same guiding principles as our previously proposed theory of MSG. The basic postulates are that the flow stress is governed by the Taylor hardening model and that the essential structure of conventional plasticity such as normality is retained.

(2) For illustration purposes, we have applied the TNT plasticity to micro-bending, micro-torsion, void growth, cavitation instability and particle-reinforced composites in this paper. We have shown that the TNT theory gives practically identical predictions as the MSG theory. The constitutive equations of TNT are similar to the classical plasticity theories, which is significantly simpler than a higher-order theory such as MSG, and may have advantage in practical applications.

(3) We have shown that the TNT theory gives predictions which are in agreement with experimental results obtained from micro-indentation, micro-torsion and micro-bending tests.

Acknowledgements

The work of H.G. was supported by the NSF through Grant CMS-9820988. The work of Y.H. was supported by the NSF through Grant CMS-9896285 and by the NSF of China.

References

Acharya, A., Bassani, J.L., 2000. Lattice incompatibility and a gradient theory of crystal plasticity. J. Mech. Phys. Solids 48, 1565–1595.

Aifantis, E.C., 1984. On the microstructural origin of certain inelastic models. Trans ASME J. Engng. Mater. Technol. 106, 326–330.

Arsenlis, A., Parks, D.M., 1999. Crystallographic aspects of geometrically-necessary and statistically-stored dislocation density. Acta Mater. 47, 1597–1611.

Ashby, M.F., 1970. The deformation of plastically non-homogeneous alloys. Phil. Mag. 21, 399–424.

Bazant, Z.P., 1986. Mechanics of distributed cracking. Appl. Mech. Rev. 26, 675–705.

Bazant, Z.P., Belytschko, T.B., Chang, T.B., 1984. Continuum theory for strain softening. ASCE J. Engng. Mech. 110, 1666–1691.

Bazant, Z.P., Lin, F.B., 1988. Non-local yield limit degradation. Int. J. Numer. Mech. Engng. 26, 1805–1823.

Bishop, J.F.W., Hill, R., 1951a. A theory of plastic distortion of a polycrystalline aggregate under combined stresses. Phil. Mag. 42, 414.

Bishop, J.F.W., Hill, R., 1951b. A theoretical derivation of the plastic properties of a polycrystalline face-centered metal. Phil. Mag. 42, 1298.

Bishop, R.F., Hill, R., Mott, N.F., 1945. The theory of indentation and hardness tests. Proc. Phys. Soc. 57, 147–159.

Chen, E.P., 1999. Non-local effects on dynamic damage accumulation in brittle solids. Int. J. Num. Meth. Geomech. 23, 1–22.

Cottrell, A.H., 1964. The Mechanical Properties of Matter. Wiley, New York, p. 277.

Dai, H., Parks, D.M., 2000. Geometrically-necessary dislocation density in continuum crystal plasticity theory and FEM implementation, in press.

Dauskardt, R., Lane, M., Ma, Q., Krishna, N., 1998. Adhesion and debonding of multi-layer thin film structures. Engng. Fract. Mech. 61, 141–162.

de Borst, R., Muhlhaus, H.-B., 1992. Gradient-dependent plasticity: formulation and algorithmic aspects. Int. J. Numer. Met. Engng. 35, 521–539.
De Guzman, M.S., Neubauer, G., Flinn, P., Nix, W.D., 1993. The role of indentation depth on the measured hardness of materials. Materials Research Symposium Proceedings 308, 613–618.
Elssner, G., Korn, D., Ruehle, M., 1994. The influence of interface impurities on fracture energy of UHV diffusion bonded metal–ceramic bicrystals. Scripta Metall. Mater. 31, 1037–1042.
Eringen, A.C., 1981. On nonlocal plasticity. Int. J. Eng. Sci. 19, 1461–1474.
Eringen, A.C., 1983. Theories of nonlocal plasticity. Int. J. Eng. Sci. 21, 741–751.
Fleck, N.A., Hutchinson, J.W., 1993. A phenomenological theory for strain gradient effects in plasticity. J. Mech. Phys. Solids 41, 1825–1857.
Fleck, N.A., Hutchinson, J.W., 1997. Strain gradient plasticity. In: Hutchinson, J.W., Wu, T.Y. (Eds.), Advances in Applied Mechanics. vol. 33. Academic Press, New York, pp. 295–361.
Fleck, N.A., Muller, G.M., Ashby, M.F., Hutchinson, J.W., 1994. Strain gradient plasticity: theory and experiment. Acta. Metallurgica et Materialia 42, 475–487.
Gao, H., Huang, Y., Nix, W.D., Hutchinson, J.W., 1999a. Mechanism-based strain gradient plasticity – I. Theory. J. Mech. Phys. Solids 47, 1239–1263.
Gao, H., Huang, Y., Nix, W.D., 1999b. Modeling plasticity at the micrometer scale. Naturwissenschaften 86, 507–515.
Gurson, A.L., 1977. Continuum theory of ductile rupture by void nucleation and growth: part I – yield criteria and flow rules for porous ductile media. J. Eng. Mater. Technol. 99, 2–15.
Hill, R., 1950. Mathematical Theory of Plasticity. Oxford University Press, Oxford, England.
Huang, Y., 1991. Accurate dilatation rate for spherical voids in triaxial stress fields. J. Appl. Mech. 58, 1084–1086.
Huang, Y., Hutchinson, J.W., Tvergaard, V., 1991. Cavitation instabilities in elastic–plastic solids. J. Mech. Phys. Solids 39, 223–241.
Huang, Y., Gao, H., Hwang, K.C., 1999. Strain-gradient plasticity at the micron scale. In: Ellyin, F., Provan, J.W. (Eds.), Progress in Mechanical Behavior of Materials. vol. III. pp. 1051–1056.
Huang, Y., Gao, H., Nix, W.D., Hutchinson, J.W., 2000a. Mechanism-based strain gradient plasticity – II. Analysis. J. Mech. Phys. Solids 48, 99–128.
Huang, Y., Xue, Z., Gao, H., Nix, W.D., Xia, Z.C., 2000b. A study of micro-indentation hardness tests by mechanism-based strain gradient plasticity, J. Mat. Res., in press.
Hutchinson, J.W., 1997. Linking scales in mechanics. In: Karihaloo, B.L., Mai, Y.-W., Ripley, M.I., Ritchie, R.O. (Eds.), Advances in Fracture Research. Pergamon Press, New York, pp. 1–14.
Kocks, U.F., 1970. The relation between polycrystal deformation and single crystal deformation. Metall. Trans. 1, 1121–1144.
Koiter, W.T., 1964. Couple stresses in the theory of elasticity, I and II. Proc. K. Ned. Akad. Wet. (B) 67, 17–44.
Kroener, E., 1962. Dislocations and continuum mechanics. Appl. Mech. Rev. 15, 599–606.
Lloyd, D.J., 1994. Particle reinforced aluminum and magnesium matrix composites. Int. Mater. Rev. 39, 1–23.
Ma, Q., Clarke, D.R., 1995. Size dependent hardness in silver single crystals. J. Mater. Res. 10, 853–863.
McElhaney, K.W., Vlassak, J.J., Nix, W.D., 1998. Determination of indenter tip geometry and indentation contact area for depth-sensing indendation experiments. J. Mater. Res. 13, 1300–1306.
McLean, D., 1962. Mechanical Properties of Metals. Wiley, New York.
Mindlin, R.D., 1964. Micro-structure in linear elasticity. Arch. Ration. Mech. Anal. 16, 51–78.
Nan, C.-W., Clarke, D.R., 1996. The influence of particle size and particle fracture on the elastic/plastic deformation of metal matrix composites. Acta Mat. 44, 3801–3811.
Needleman, A., Tvergaard, V., Hutchinson, J.W., 1992. Void growth in plastic solids. In: Argon, A.S. (Ed.), Topics in Fracture and Fatigue. Springer, New York, pp. 145–178.
Nix, W.D., 1989. Mechanical properties of thin films. Metall. Trans. 20A, 2217–2245.
Nix, W.D., Gao, H., 1998. Indentation size effects in crystalline materials: a law for strain gradient plasticity. J. Mech. Phys. Solids 46, 411–425.
Nix, W.D., Gibeling, J.C., 1985. Mechanism of Time-dependent Flow and Fracture of Metals. Metals/Materials Technology Series 8313-004. ASM, Metals Park, OH.
Nye, J.F., 1953. Some geometrical relations in dislocated crystal. Acta Metall. 1, 153–162.
Parks, D.M., 1999. Private communication.
Pijaudier-Cabot, G., Bazant, Z.P., 1987. Nonlocal damage theory. ASCE J. Eng. Mech. 10, 1512–1533.
Poole, W.J., Ashby, M.F., Fleck, N.A., 1996. Microhardness of annealed and work-hardened copper polycrystals. Scripta Metall. Mater. 34, 559–564.
Rice, J.R., 1970. On the structure of stress–strain relations for time-dependent plastic deformation in metals. J. Appl. Mech. 34, 728–737.
Rice, J.R., 1971. Inelastic constitutive relations for solids: an internal-variable theory and its application to metal plasticity. J. Mech. Phys. Solids 19, 433–455.

Rice, J.R., Tracy, D.M., 1969. On the ductile enlargement of holes in triaxial stress fields. J. Mech. Phys. Solids 17, 201–217.
Stelmashenko, N.A., Walls, M.G., Brown, L.M., Milman, Y.V., 1993. Microindentation on W and Mo oriented single crystals: an STM study. Acta Metallurgica et Materialia 41, 2855–2865.
Stolken, J.S., Evans, A.G., 1998. A microbend test method for measuring the plasticity length scale. Acta Mater. 46, 5109–5115.
Stromberg, L., Ristinmaa, K., 1996. FE-formulation of a nonlocal plasticity theory. Comp. Met. Appl. Mech. Eng. 136, 127–144.
Toupin, R.A., 1962. Elastic materials with couple stresses. Arch. Ration. Mech. Anal. 11, 385–414.
Tvergaard, V., 1990. Material failure by void growth to coalescence. Adv. Appl. Mech. 27, 83–147.
Zbib, H., Aifantis, E.C., 1989a. On the localization and postlocalization behavior of plastic deformation. Part I. On the initiation of shear bands. Res. Mech. 23, 261–277.
Zbib, H., Aifantis, E.C., 1989b. On the localization and postlocalization behavior of plastic deformation. Part II. On the evolution and thickness of shear bands. Res. Mech. 23, 279–292.
Zbib, H., Aifantis, E.C., 1989c. On the localization and postlocalization behavior of plastic deformation. Part III. On the structure and velocity of Portevin-Le Chatelier bands. Res. Mech. 23, 293–305.